Transient Higgs oscillations and high-order nonlinear light-Higgs coupling in a terahertz wave driven NbN superconductor

Zi-Xiao Wang [1,*] Jie-Ran Xue [1,*] Hong-Kai Shi,[2] Xiao-Qing Jia,[2] Tong Lin,[1] Li-Yu Shi,[1] Tao Dong,[1,†]
Fa Wang [1,‡] and Nan-Lin Wang[1,3,§]

[1]*International Center for Quantum Materials, School of Physics, Peking University, Beijing 100871, China*
[2]*School of Electronic Science and Engineering, Nanjing University, Nanjing 210093, China*
[3]*Beijing Academy of Quantum Information Sciences, Beijing 100913, China*

We study the nonlinear optical response in a superconducting NbN thin film with a strong terahertz (THz) wave. In. addition to the expected third-harmonic generation, we observe a transient oscillation which softens in frequency with temperature increasing towards the superconducting transition temperature T_c. We identify this feature as transient Higgs oscillation. To verify this proposal, we introduce a time-frequency resolved technique, a spectrogram for visualizing the THz spectrum. The dynamic decaying behavior of the oscillation is observed, which is consistent with the theoretical expectation of intrinsic Higgs oscillation. Moreover, we observe a higher-order nonlinear optics effect, i.e., fifth-harmonic generation, which we assign to the higher-order coupling between the Higgs mode and electromagnetic field.

With the recent development of state-of-the-art strong-field terahertz (THz) spectroscopy, it becomes possible to study linear or nonlinear electromagnetic wave-matter coupling in a regime that was not accessible before [1,2]. Since the energy scale of THz light is in the range of meV, it can gently excite quantum materials without destroying their electronic orders. Unlike the infrared excitation at higher energies, the THz experiments provide more direct information about the low-lying excitations or ground-state properties of quantum materials.

Among the most appealing applications of strong-field THz electromagnetic waves is to excite and probe collective modes of matter, such as the Higgs mode in a superconductor [3–20]. The Higgs mode emerges as a result of the spontaneous breaking of U(1) symmetry in the superconducting state, which is characterized by a Mexican-hat-shaped free energy potential. In principle, there are two kinds of collective excitations associated with this symmetry breaking order: a phase excitation azimuthally around the brim of the Mexican hat; and an amplitude excitation along the radial direction of the Mexican hat. For a superconductor, the phase part, which is referred to as the Nambu-Goldstone mode, is screened by long-range Coulomb interactions between charges and shifted up to the plasma frequency by the Anderson-Higgs mechanism. The amplitude part is called the Higgs mode, which is a massive mode with an energy at the superconducting energy gap 2Δ. The Higgs mode in a superconductor is an analogy to the Higgs boson in particle physics [5,21,22].

Since the Higgs mode does not possess an electric or magnetic dipole moment, it does not couple linearly to light. This limitation makes it difficult to be detected, except for some special cases, e.g., the coexistence of superconductivity and charge-density wave order that makes the Higgs mode Raman active and detectable by Raman scattering experiments [23–27]. In recent years, with the development of strong-field THz technology, the Higgs mode can be excited and probed by two different ways. One is to quench the superconducting system by a single-cycle THz pump pulse that brings it out of the equilibrium state. Then, the order parameter starts to oscillate at the new equilibrium state with the Higgs mode frequency 2Δ that can be detected by a time-domain THz probe measurement [9,28]. The other way is to drive the system periodically with a multicycle THz pulse [10,14,17,20]. In the context of Ginzburg-Landau theory, the lowest-order coupling between the Higgs mode H and electromagnetic field $\mathbf{A}(\omega)$ is $\mathbf{A}^2(\omega)H$. This nonlinear coupling of light to the superconducting condensate induces oscillation of the order parameter at twice the driving frequency 2ω. This nonlinear coupling can also induce higher-order third-harmonic generation (THG) currents $j^{(3)}(t)$, resulting from the driven oscillations of the Higgs mode, i.e., $j^{(3)}(3\omega) \propto \mathbf{A}(\omega)H(2\omega)$. With the effective 2ω driving frequency approaching towards the energy of the Higgs mode 2Δ, a resonance in the gap oscillation occurs and consequently in the THG intensity as well. This behavior has been observed in the transmitted electric field [10]. Although there have been arguments that, in addition to the Higgs mode, the charge-density fluctuation or pair breaking also induces the THG with a similar resonant character at $2\omega = 2\Delta$ [29,30], subsequent polarization-resolved terahertz studies showed that the Higgs mode makes a dominant contribution to the THG far exceeding the charge-density fluctuation contribution in the NbN superconductor [13,31].

---

*Those authors contributed equally to this work.

†taodong@pku.edu.cn

‡wangfa@pku.edu.cn

§nlwang@pku.edu.cn
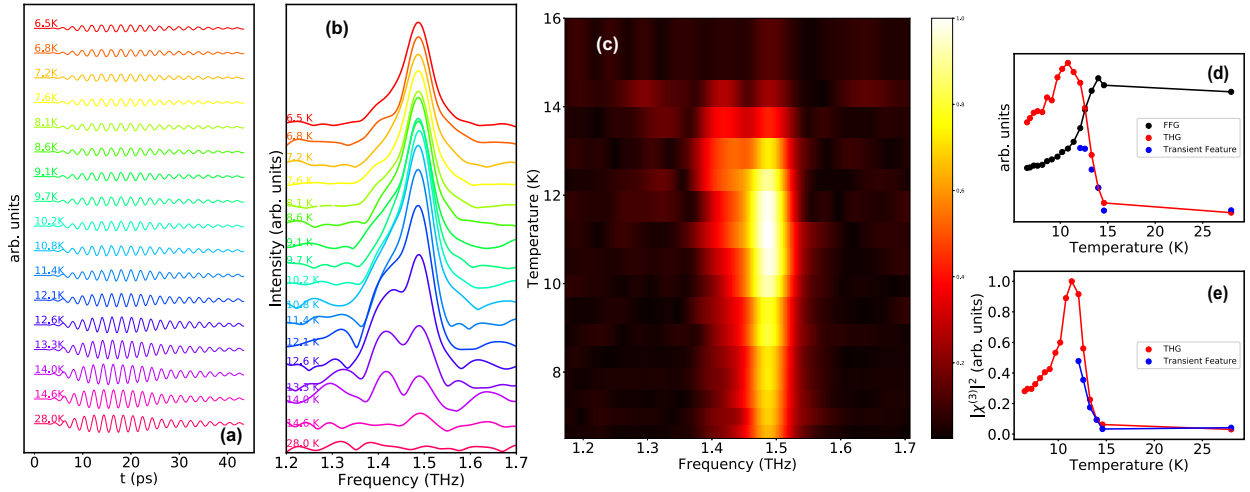
FIG. 1. Temperature dependence of third-harmonic generation in NbN. (a) Strong-field THz transmission electric fields of the NbN crystal measured from the superconducting state to normal state. (b) The spectra in frequency domain around 1.5 THz via Fourier transformation of (a). (c) Temperature-dependent intensity map in the frequency domain extracted from (b). (d) Spectral weight of FFG, THG, and transient feature (black, red, and blue solid circles, respectively) vs temperature. (e) The normalization of THG and transient feature after considering the screening effect.

In this Letter, we study the optical response in the superconductor NbN under multicycle THz driving pulses. We observed a weak oscillation peak feature close to the THG feature, which shifts towards lower energy with increasing temperature. In light of the theoretical analysis, we identify the feature as transient Higgs oscillation. It means that the quench dynamics is present in the THz driving experiment. To characterize the time evolution of the transient feature and the THG feature, we introduce the Gabor transform technique to analyze the data. We find that transient Higgs oscillation decays faster than THG oscillation, which is consistent with our theoretical prediction. Furthermore, we identify a fifth-harmonic generation (FHG), which we assign to the higher-order coupling $\mathbf{A}(\omega)^4 H$ between the Higgs mode H and electromagnetic field $\mathbf{A}(\omega)$.

A superconducting 50-nm-thick NbN thin film grown on an MgO substrate was used for the experiment [32]. The nonlinear high-harmonic generation spectra were measured in a home-built high-field terahertz transmission spectroscopy system. The high-field THz wave was generated by the tilted-pulse-front method on a LiNbO$_3$ crystal. More details about the light path are provided in the Supplemental Material [33].

To investigate the nonlinear optical response of the strong-field terahertz THG signal, we put 0.5-THz bandpass filters (BPFs) before the NbN film. Then, the single-cycle broadband THz light is reshaped into a multicycle narrow-band light around 0.5 THz with a maximum peak electric field ∼4.6 kV/cm. We measured the time-domain THz transmission electric field of the NbN film with $T_c = 15$ K by increasing the temperature from the superconducting state to the normal state. The time traces at selected temperatures are shown in Fig. 1(a). The Fourier transformed spectra between 1.2 and 1.7 THz in the frequency domain $|\tilde{E}(\omega)|$ are presented in Fig. 1(b). In the low-temperature superconducting state, there is a visible THG peak at 1.5 THz. As the temperature rises, the THG signal increases and reaches maximum under resonant conditions with 0.5 THz at 11.4 K. Then, it recedes and

disappears above T_c, which confirms that the THG signal is linked with superconductivity. Figure 1(c) shows the intensity map extracted from Fig. 1(b). The THG peak at 1.5 THz does not show any shift in frequency with temperature increasing from the lowest measurement temperature at 6 K to T_c. The spectral weights of fundamental frequency generation (FFG) and THG shown in Fig. 1(d) are obtained by integration around 0.5 and 1.5 THz, respectively, defined as SW(ω_0) = $\int_{\omega_0-\Delta\omega}^{\omega_0+\Delta\omega} E(\omega)d\omega$ with $\Delta\omega = 0.1$ THz. With the increase of temperature, the FFG signal monotonically increases due to the enhancement of transmittance, while the THG signal increases first, decreases subsequently, and finally vanishes. Taking the transmitted FFG intensity as an estimate for the electric field inside the superconducting thin film [17], we can correct for the screening effect and obtain the third-order susceptibility $|\chi^{(3)}|^2$ from the normalized THG intensity by the transmitted FFH intensity, as displayed in Fig. 1(e). We notice that a discernible peak emerges as the temperature rises over 10 K and a redshift of this peak with temperature occurs, as seen in Figs. 1(b) and 1(c). It is attributed to the softening of the transient Higgs oscillation and will be explained in detail later. Its spectral weight and the normalized spectral weight by FFG as well are shown as blue solid circles in Figs. 1(d) and 1(e), respectively.

As a third-order nonlinear optical process, THG is proportional to the electric field intensity to the third power. Figure 2 shows the result of fluence-dependent measurements at 6.5 K. We put two THz wire grid polarizers (WGPs) after a 0.5-THz BPF to control the intensity of the incoming electric field. Due to the Malus law $I \propto |\cos^2(\theta)|$ where θ is the phase difference between two WGP directions, a variety of electric fields can be realized by rotating the polarization direction of one THz wire grid polarizer. Figures 2(a) and 2(b) present time- and frequency-domain THz electric fields $E(t)$ and $|\tilde{E}(\omega)|$ as a function of fluence. Figure 2(c) shows the details about the THG peak at 1.5 THz. The spectral weight of FFG and THG versus incoming THz light is shown in Fig. 2(d), where the
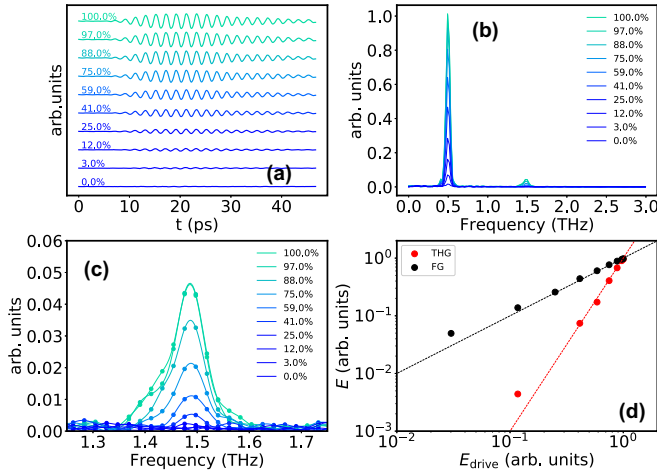
FIG. 2. Power dependence of third-harmonic generation in NbN. (a) THz electric field transmitted through NbN at different powers of an incoming electric field. (b) The frequency-domain spectra via Fourier transformation of (a). (c) An enlarged view of the details about THG at 1.5 THz. (d) The spectral weight of FFG and THG vs the incoming electric field. The black and red lines are the fitting curves by the linear and the third power function, respectively.

solid black and red circles are the spectral weight, extracted from integration around 0.5 and 1.5 THz in Fig. 2(b), respectively. The relation between THG and incoming THz light agrees well with the expected third power law: $E^{\mathrm{THG}}(3\omega) \propto E^3(\omega)$. The black and red dashed lines are fitting curves to the linear and third power functions, respectively.

As mentioned above, we observe a weak oscillation feature around 1.5 THz in Figs. 1(b) and 1(c). With the temperature increasing, the frequency of the peak at 1.5 THz remains unchanged, while the peak below 1.5 THz shows a redshift. We identify these two oscillations as the third-harmonic generation and the transient Higgs oscillation, respectively. The frequency of forced vibration is only related to the driving frequency ω, thus the frequency of the THG does not depend on temperature. In contrast, the redshifted transient Higgs oscillation is not only related to the unchanged driving frequency ω, but also depends on the intrinsic Higgs mode energy $2\Delta(T)$ which softens with increasing temperature. When a multicycle strong-field THz pulse arrives, the system is nonadiabatically pushed into a nonequilibrium state and will evolve towards the time-periodically forced oscillation state. At the arrival of the pump pulse, the transient Higgs oscillation should be predominant, and its oscillation frequency is temperature dependent. As the system approaches a stable periodically driven state, the transient Higgs oscillation decays gradually while the THG persists and becomes predominant, whose frequency remains unchanged with a change of temperature. The transient Higgs signal disappears before the temperature reaches T_c since the resonant enhancement is suppressed when $2\Delta(T)$ moves out of the narrow bandwidth of the incident pump field. The scenario proposed above is supported by our theoretical calculation based on the Anderson pseudospin precession picture. This process can also be understood by the analogy of a forced harmonic oscillator, which has nonlinear coupling to an external force. Both the transient oscillation

and the third-harmonic generation can be observed in the harmonic oscillator system. (See more details in the Supplemental Material [33].) We note that, in a reported work on NbN [10], the authors did not resolve two separate features but indicated a redshift of the THG peak when the temperature is elevated to T_c. The observation is somewhat different from the present work. Nevertheless, the softening of the transient Higgs oscillation is likely the reason for the observed redshift of THG, which might be caused by the limited frequency resolution.

To clarify the above proposal, we introduce the time-frequency distribution spectrogram to separate the transient Higgs oscillation and THG oscillation (see more details in the Supplemental Material [33]). A spectrogram is an analysis tool that is used to characterize signals whose spectral content is varying in time [34]. The techniques are called frequency-resolved optical gating (FROG). It is widely used in femtosecond laser pulse measurements, and a FROG trace visually displays the frequency versus time delay. Here, we use it to analyze the time-domain terahertz spectrum. The time-frequency-resolved result is extracted from a time-domain spectrum with different time-delay gating windows by

$$S(\omega, \tau) \equiv \left| \int_{-\infty}^{\infty} E(t)g(t - \tau)\exp(-\mathbf{i}\omega t)dt \right|^2, \quad (1)$$

where $g(t - \tau)$ is the gating window function. When a Gaussian function is chosen as the gating window function $g(t - \tau) = e^{-[(t-\tau)/T]^2}$ with T the time window, the spectrogram is equivalent to the so-called Gabor transformation which was also often used for time-frequency analysis [35]. We choose $T = 6$ ps in the integration. where the gating function is set as the Gaussian function $g(t - \tau) = e^{-[(t-\tau)/T]^2}$. We checked that the effect is small if a different value is used for the time window. Figure 3 shows the time-frequency spectrogram derived from the time-domain THz spectrum at 12.6 K. The experimental and theoretical results are as shown in Figs. 3(a) and 3(b) and Figs. 3(c) and 3(d), respectively (see Supplemental Material for details [33]). We notice that the main peak at 0.5 THz is free of phase or frequency modulation as shown in Figs. 3(a) and 3(c). If the signal around 1.5 THz was entirely THG and no other components, it should also be free of phase or frequency modulation, the same as the main peak at 0.5 THz. However, a positive chirp, i.e., longer times corresponding to higher frequencies in THG, is observed, as shown in Figs. 3(b) and 3(d). It demonstrates that there is another nonlinear optical response besides THG, that is, the transient Higgs oscillation. The theoretical and experimental results are very similar. The frequency of the transient Higgs oscillation and THG is indicated in Figs. 3(b) and 3(d) by the dotted black lines (the temperature mismatch in experiment and theoretical calculation may be due to the too simple model we adopt to simulate the time evolution). The spectrum can be divided into two peaks by different delay times τ of $g(t - \tau)$, shown in Figs. 3(b) and 3(d) by the dashed lines from blue to red. The global and frequency-domain spectra with different gating windows are shown in Fig. 3(e) experimentally and Fig. 3(f) theoretically. The transient Higgs oscillation decays faster than THG. Since transient Higgs oscillation is observed in the driving experiment, the results may provide additional
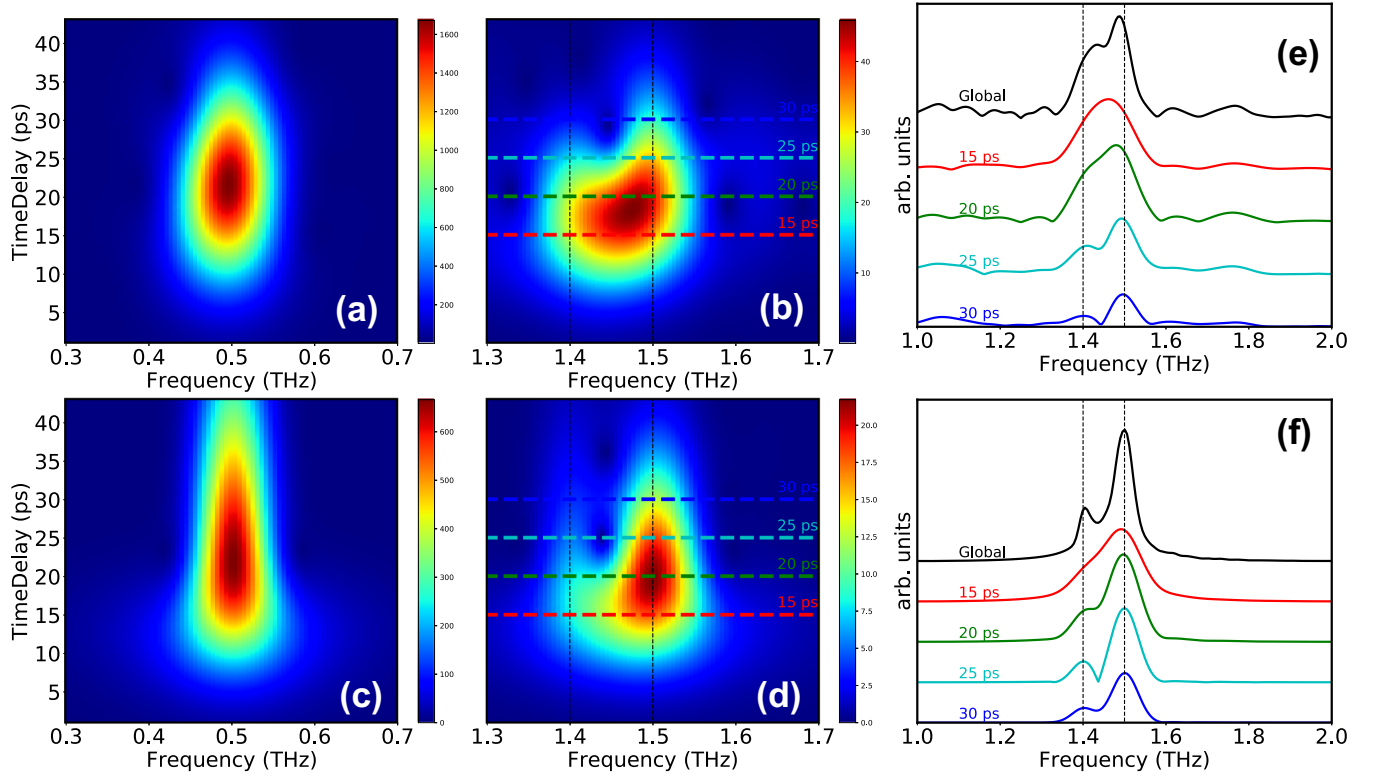
FIG. 3. Spectrogram traces for frequency-resolved THG by Gabor transformation. The traces are shown as contour plots, with red regions indicating higher intensity [with (a), (b) experimental results and (c), (d) theoretical results]. Both traces correspond to identical Gaussian power spectra, but with different spectral phase profiles. FFG, bandwidth limited, as shown in (a), (c); THG, upchirp with cubic spectral phase, as shown in (b) and (d). (e), (f) The division of the Fourier transform spectrum: From red to blue lines are extracted from the dashed lines in (b) and (d).

support that the THG signal is contributed dominantly from the Higgs excitation rather than the charge-density fluctuation.

We now present another striking and interesting observation in our THz pulse driving measurement. We observed a weak high-order (fifth-order) nonlinear optics effect when we placed 0.4-THz bandpass filters before the NbN sample. Here, a multicycle, narrow-band, 0.4-THz pulse is generated and employed as the fundamental frequency light. Figure 4(a) shows the measured time-domain THz transmission electric field of the NbN film at 6.8 K in the superconducting state. The Fourier transformed spectrum is shown in Fig. 4(b). We observed a weak but well-recognizable FHG peak around 2.0 THz in addition to the stronger THG signal at 1.2 THz. As the temperature rises, the THG and FHG signals further weaken and totally vanish when the sample goes into a normal state. We also observed a similar FHG with a driving fundamental frequency of 0.3 THz, but much weaker strength (the result is shown in the Supplemental Material [33]). However, we cannot resolve such an FHG signal when the driving fundamental frequency is 0.5 THz at 6.8 K.

Since the frequencies of FHG for 0.3, 0.4, and 0.5 THz incoming driving waves are 1.5, 2.0, and 2.5 THz, respectively, the relatively strong FHG signal is likely linked to the fact that 2.0 THz is closer to the resonant energy of 2Δ. We assign FHG to the higher-order coupling $\mathbf{A}^4(\omega)H$ between Higgs mode H and electromagnetic field $\mathbf{A}(\omega)$. This coupling will induce driven oscillations of the Higgs mode at frequency 4ω whose amplitude will be largest when 4ω matches the

intrinsic Higgs mode energy $2\Delta(T)$, and it will further produce a FHG component of current $j^{(5)}(5\omega) \propto \mathbf{A}(\omega)H(4\omega)$. Our theoretical modeling can indeed reproduce the observed FHG result. Detailed information is presented in the Supplemental Material [33].

To summarize, we observe transient Higgs oscillation around the THG oscillation and a redshift behavior for this transient oscillation feature as temperature increases. We
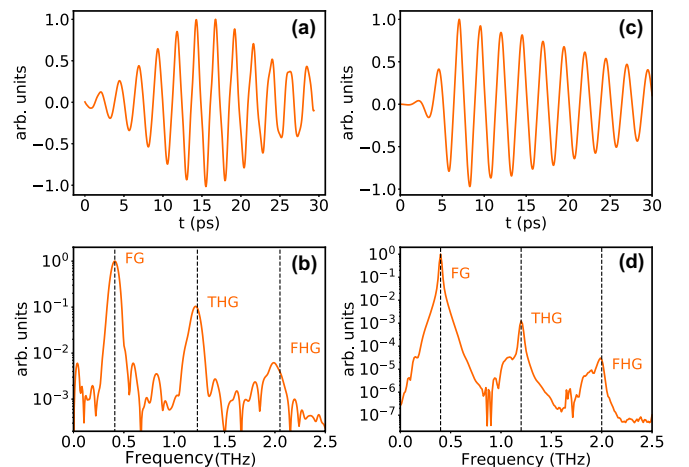
FIG. 4. The fifth-harmonic generation in NbN. (a) (b) Strong-field and 0.4-THz field transmitted through NbN at 6.8 K. (c), (d) Similar results from theoretical calculations.

propose a scenario where the quench dynamics is still present in the driving experiment to explain this feature. We confirm this assumption by a time-frequency distribution spectrogram. The temperature-dependence signal decays fast, while the strict THG signal at 3ω oscillates at a much longer time delay. We also observe a weak but clearly discernible fifth-harmonic generation in a thin-film NbN sample, which we assign to the higher-order coupling between the Higgs mode and electromagnetic field.

[1] J. Orenstein, Phys. Today **65** (9), 44 (2012).

[2] C. Giannetti, M. Capone, D. Fausti, M. Fabrizio, F. Parmigiani, and D. Mihailovic, Adv. Phys. **65**, 58 (2016).

[3] P. W. Anderson, Phys. Rev. **130**, 439 (1963).

[4] P. W. Higgs, Phys. Rev. Lett. **13**, 508 (1964).

[5] C. M. Varma, J. Low Temp. Phys. **126**, 901 (2002).

[6] E. A. Yuzbashyan, O. Tsyplyatyev, and B. L. Altshuler, Phys. Rev. Lett. **96**, 097005 (2006).

[7] D. Podolsky, A. Auerbach, and D. P. Arovas, Phys. Rev. B **84**, 174522 (2011).

[8] Y. Barlas and C. M. Varma, Phys. Rev. B **87**, 054503 (2013).

[9] R. Matsunaga, Y. I. Hamada, K. Makise, Y. Uzawa, H. Terai, Z. Wang, and R. Shimano, Phys. Rev. Lett. **111**, 057002 (2013).

[10] R. Matsunaga, N. Tsuji, H. Fujita, A. Sugioka, K. Makise, Y. Uzawa, H. Terai, Z. Wang, H. Aoki, and R. Shimano, Science **345**, 1145 (2014).

[11] N. Tsuji and H. Aoki, Phys. Rev. B **92**, 064508 (2015).

[12] D. Pekker and C. Varma, Annu. Rev. Condens. Matter Phys. **6**, 269 (2015).

[13] R. Matsunaga, N. Tsuji, K. Makise, H. Terai, H. Aoki, and R. Shimano, Phys. Rev. B **96**, 020505(R) (2017).

[14] F. Yang and M. W. Wu, Phys. Rev. B **100**, 104513 (2019).

[15] T. Cui, X. Yang, C. Vaswani, J. Wang, R. M. Fernandes, and P. P. Orth, Phys. Rev. B **100**, 054504 (2019).

[16] L. Schwarz and D. Manske, Phys. Rev. B **101**, 184519 (2020).

[17] H. Chu, M.-J. Kim, K. Katsumi, S. Kovalev, R. D. Dawson, L. Schwarz, N. Yoshikawa, G. Kim, D. Putzky, Z. Z. Li, H. Raffy, S. Germanskiy, J.-C. Deinert, N. Awari, I. Ilyakov, B. Green, M. Chen, M. Bawatna, G. Cristiani, G. Logvenov *et al.*, Nat. Commun. **11**, 1793 (2020).

[18] L. Schwarz, B. Fauseweh, N. Tsuji, N. Cheng, N. Bittner, H. Krull, M. Berciu, G. S. Uhrig, A. P. Schnyder, S. Kaiser, and D. Manske, Nat. Commun. **11**, 287 (2020).

[19] R. Shimano and N. Tsuji, Annu. Rev. Condens. Matter Phys. **11**, 103 (2020).

[20] S. Kovalev, T. Dong, L.-Y. Shi, C. Reinhoffer, T.-Q. Xu, H.-Z. Wang, Y. Wang, Z.-Z. Gan, S. Germanskiy, J.-C. Deinert, I. Ilyakov, P. H. M. van Loosdrecht, D. Wu, N.-L. Wang, J. Demsar, and Z. Wang, Phys. Rev. B **104**, L140505 (2021).

[21] Y. Nambu, Phys. Rev. Lett. **4**, 380 (1960).

[22] G. E. Volovik and M. A. Zubkov, J. Low Temp. Phys. **175**, 486 (2014).

[23] R. Sooryakumar and M. V. Klein, Phys. Rev. Lett. **45**, 660 (1980).

[24] P. B. Littlewood and C. M. Varma, Phys. Rev. Lett. **47**, 811 (1981).

[25] P. B. Littlewood and C. M. Varma, Phys. Rev. B **26**, 4883 (1982).

[26] M.-A. Méasson, Y. Gallais, M. Cazayous, B. Clair, P. Rodière, L. Cario, and A. Sacuto, Phys. Rev. B **89**, 060503(R) (2014).

[27] T. Cea and L. Benfatto, Phys. Rev. B **90**, 224515 (2014).

[28] F. Giorgianni, T. Cea, C. Vicario, C. P. Hauri, W. K. Withanage, X. Xi, and L. Benfatto, Nat. Phys. **15**, 341 (2019).

[29] T. Cea, C. Castellani, and L. Benfatto, Phys. Rev. B **93**, 180507(R) (2016).

[30] T. Cea, P. Barone, C. Castellani, and L. Benfatto, Phys. Rev. B **97**, 094516 (2018).

[31] N. Tsuji and Y. Nomura, Phys. Rev. Research **2**, 043029 (2020).

[32] L. Kang, B. B. Jin, X. Y. Liu, X. Q. Jia, J. Chen, Z. M. Ji, W. W. Xu, P. H. Wu, S. B. Mi, A. Pimenov, Y. J. Wu, and B. G. Wang, J. Appl. Phys. **109**, 033908 (2011).

[33] See Supplemental Material at http://link.aps.org/supplemental/10.1103/PhysRevB.105.L100508 for the details about the light path, spectra in equilibrium and numerical simulation.

[34] A. M. Weiner, *Ultrafast Optics* (Wiley, Hoboken, NJ, 2009).

[35] H. G. Feichtinger and T. Strohmer, *Gabor Analysis and Algorithms: Theory and Applications* (Springer, Berlin, 2012).